Spatial Distortion of Vibration Modes via Magnetic Correlation of Impurities

F. S. Krasniqi,[1,2,*] Y. Zhong,[1,2,3,†] S. W. Epp,[1,4,3] L. Foucar,[1,2] M. Trigo,[5] J. Chen,[5] D. A. Reis,[5] H. L. Wang,[6]
J. H. Zhao,[6] H. T. Lemke,[7,‡] D. Zhu,[7] M. Chollet,[7] D. M. Fritz,[7] R. Hartmann,[8] L. Englert,[9,§]
L. Strüder,[1,8,9,10] I. Schlichting,[1,2] and J. Ullrich[1,4,‖]

[1]*Max Planck Advanced Study Group at CFEL/DESY, Notkestraße 85, 22607 Hamburg, Germany*
[2]*Max-Planck-Institut für medizinische Forschung, Jahnstraße 29, 69120 Heidelberg, Germany*
[3]*Max Planck Institute for the Structure and Dynamics of Matter,*
Luruper Chaussee 149, Building 99 (CFEL), 22761 Hamburg, Germany
[4]*Max Planck Institute for Nuclear Physics, Saupfercheckweg 1, 69117 Heidelberg, Germany*
[5]*Stanford PULSE and SIMES Institutes, SLAC National Accelerator Laboratory, Menlo Park, California 94025, USA*
[6]*State Key Laboratory of Superlattices and Microstructures, Institute of Semiconductors, Chinese Academy of Sciences,*
P.O. Box 912, Beijing 100083, People's Republic of China
[7]*Linac Coherent Light Source, SLAC National Accelerator Laboratory, Menlo Park, California 94025, USA*
[8]*PNSensor GmbH, Römerstraße 28, 80803 München, Germany*
[9]*Max Planck Institute for Extraterrestrial Physics, Giessenbachstrasse 1, 85748 Garching, Germany*
[10]*Max-Planck-Society Semiconductor Laboratory, Otto-Hahn-Ring 6, 81739 München, Germany*

Long wavelength vibrational modes in the ferromagnetic semiconductor $Ga_{0.91}Mn_{0.09}As$ are investigated using time resolved x-ray diffraction. At room temperature, we measure oscillations in the x-ray diffraction intensity corresponding to coherent vibrational modes with well-defined wavelengths. When the correlation of magnetic impurities sets in, we observe the transition of the lattice into a disordered state that does not support coherent modes at large wavelengths. Our measurements point toward a magnetically induced broadening of long wavelength vibrational modes in momentum space and their quasilocalization in the real space. More specifically, long wavelength vibrational modes cannot be assigned to a single wavelength but rather should be represented as a superposition of plane waves with different wavelengths. Our findings have strong implications for the phonon-related processes, especially carrier-phonon and phonon-phonon scattering, which govern the electrical conductivity and thermal management of semiconductor-based devices.

Impurity atoms play an important role in condensed matter physics, in particular, in the nature of lattice vibrations. They typically perturb the crystal Hamiltonian by producing an alternation in the kinetic energy of the ions due to a mass difference relative to the host and by modifying the force constants around the impurity atom [1,2]. Hence, the vibration modes are expected to be modified from their usual sinusoidal wave forms, which consequently leads to important implications for the thermal and electrical properties of the host crystal, in particular, heat conductivity and carrier mobility [3]. This is of vital importance for electronic devices whose miniaturization not only increases the processing rate but also the quantity of heat that, subsequently, might lead to large thermal loads and device failure. In the context of materials with large technological relevance, semiconductors doped with magnetic impurities, commonly known as diluted magnetic semiconductors (DMS), open up new prospects for extending the information processing and storage beyond conventional electronics by merging the long-range magnetic ordering characteristic of ferromagnets with the versatile properties of conventional

semiconductors [5,6]. The large number of magnetic impurity atoms needed to mediate the ferromagnetic coupling ($\sim 2.2 \times 10^{20}$ cm^3) will considerably affect the traveling-wave-nature of the host-crystal normal modes and phonon transport. In contrast to amorphous and disordered solids where localized and quasilocalized modes have been extensively studied and debated [1,2,7–14], the experimental work on doped semiconductors with correlated impurities remains scarce. Motivated by this fact, our objective was to observe how phonon modes in DMSs develop and evolve when magnetic moments interact with each other.

We have probed the vibrational modes of the laser excited $Ga_{0.91}Mn_{0.09}As$ by time-resolving the scattering of x-rays by phonons [15,16]. At room temperature, all components of an impulsively generated acoustic phonon pulse are traveling wave normal modes with a well-defined wave vector q. When the coupling of magnetic impurities sets in, long wavelength components of the acoustic pulse are profoundly affected. The length-scale and temperature dependence of x-ray diffraction waveforms indicate that the magnetic correlation of randomly distributed impurities

quasilocalizes the long wavelength vibrational modes. In contrast to amorphous solids and crystalline solids with heavy impurities [1,7,13], sinusoidal displacement patterns of vibrational modes are destroyed by the phase shifts at the impurity atoms rather than by the extra displacement amplitudes. The experiments were performed at the X-Ray Pump-Probe (XPP) Instrument, Linac Coherent Light Source (LCLS) X-ray FEL [17]. An ultrashort (50 fs) near-infrared (800 nm) laser pulse excites coherent acoustic phonon modes [18–21] in a 1 μm thick $Ga_{0.91}Mn_{0.09}As$ film with a Curie temperature $T_c \approx 90$ K [22]. A nominally 50 fs, 10.363 keV x-ray pulse, just below the Ga K-edge energy, is used to probe the sample (see Supplemental Material [23], Sec. A, which includes Refs. [17,22,24–30]). Any phonon-induced periodicity in the lattice with a period $\lambda_q = 2\pi/q$ will introduce sidebands to the rocking curve peak, at an angular separation $\Delta\theta \propto q$ from the Bragg peak, which oscillate at the phonon frequency ω_q (see Supplemental Material [23], Sec. B, which includes Refs. [18–21,31]).

In Figs. 1(a)–1(c), we show the time-dependent diffracted intensity from $Ga_{0.91}Mn_{0.09}As$ (004 reflection) at room temperature, probing spatial periodicities $q = 0.015 \ \pi/a$, 0.012 π/a, and 0.010 π/a, respectively, with $a = 5.673$ Å being the lattice constant of $Ga_{0.91}Mn_{0.09}As$ [32]. Distinct temporal oscillations are observed that correspond to coherent acoustic phonons at frequencies $\omega_q = 2\pi/(22 \text{ ps})$, $2\pi/(28 \text{ ps})$, and $2\pi/(31 \text{ ps})$, respectively. A Fourier transformation of the data gives the dispersion relation for the
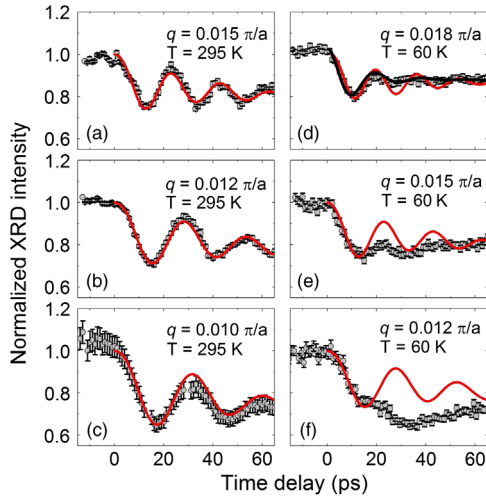

FIG. 1. Measurements (filled circles) and simulations (solid lines) of time-dependent x-ray diffracted intensity from $Ga_{0.91}Mn_{0.09}As$. Panels (a),(b),(c) show data measured at room temperature, whereas panels (d),(e),(f), at 60 K. The data have been compared with predictions of dynamical theory of x-ray diffractions that assume acoustic modes with well-defined spatial periodicity q (red solid lines). The black solid line in panel (d) represents a damped elastic wave with $q = 0.018 \ \pi/a$, $\omega_q = 2\pi/(19 \text{ ps})$ and damping time constant $\tau = 12$ ps.

longitudinal acoustic branch with a speed of sound $v_{s,\text{exp}} = 3400 \pm 400$ m/s for longitudinal acoustic modes propagating along the [001] direction, with the error bar resulting from the uncertainty in the determination of the rocking curve peak. This value is smaller than the sound velocity in GaAs, $v_{s,\text{GaAs}} = 4780 \ m/s$, due to the charge redistribution in the host crystal induced by the doping [33]. Extrapolating the spin polarized density-functional-theory calculations of elastic constants to a doping density of $x = 0.09$ [33], we obtain $v_s = 3800$ m/s, which agrees well with our experimental value. These data confirm that the probed phonon modes can be described by elastic waves having a well-defined spatial periodicity, implying that q is a good quantum number. The data compare well with simulations that model dynamical x-ray diffraction in the presence of strain. Here, the rocking curves have been calculated for a particular strain profile using the method given by Wie *et al.* [34], whereas the strain has been calculated using the model of Thomsen *et al.* [35], extended to include the lattice heating time [21,36]. The damping of the oscillations results from the dephasing due to the wave vector resolution limit of the probe beam.

The key observation of our work becomes obvious from the data depicted in Fig. 1, panels (d),(e),(f), where time-dependent x-ray diffraction intensities measured at temperature $T \approx 60$ K, but the same laser fluence as previous measurements at room temperature are reported. We show normalized intensities that probe acoustic phonon modes with spatial periodicities $q = 2\pi/\lambda_q = 0.018 \ \pi/a$, 0.015 π/a, and 0.012 π/a, respectively. The data are compared with predictions of dynamical theory of x-ray diffraction that assume acoustic modes with well-defined spatial periodicity q, similar to those used to simulate the room temperature measurements. The data measured at $q = 0.018 \ \pi/a$ resemble the form of a damped elastic wave with frequency $\omega_q = 2\pi/(19 \text{ ps})$ and a damping time constant $\tau = 12$ ps [black solid line in Fig. 1(d)], indicating that the q vector is still a good quantum number. The mode at $q = 0.015 \ \pi/a$ shows temporal oscillations at $\omega_q = 2\pi/(22 \text{ ps})$, however, with a quenched amplitude [Fig. 1(e)]. Time-dependent-diffracted intensity probing the spatial periodicity $q = 0.012 \ \pi/a$ [Fig. 1(f)] has a waveform that is markedly changed compared to that of an elastic wave with a defined q vector. In effect, only the first half period of the oscillation is observed. Evidently, the measured time-resolved diffraction depends on the ferromagnetic ordering of Mn spins; Figure 2 shows a typical critical behavior of the mode $q = 0.015 \ \pi/a$ with temperature as an example that demonstrates the dependence of measured time-dependent x-ray diffraction on the magnetic correlation of impurities. The data resemble a critical behavior around T_c, similar to that observed in the susceptibility [37,38], resistivity [39], and heat capacity [40], thus indicating a dependence on the spin-spin correlation function $\Gamma(\mathbf{S}_0, \mathbf{S}_1) = \langle \mathbf{S}_0 \mathbf{S}_1 \rangle - \langle \mathbf{S}_0 \rangle \langle \mathbf{S}_1 \rangle$. The
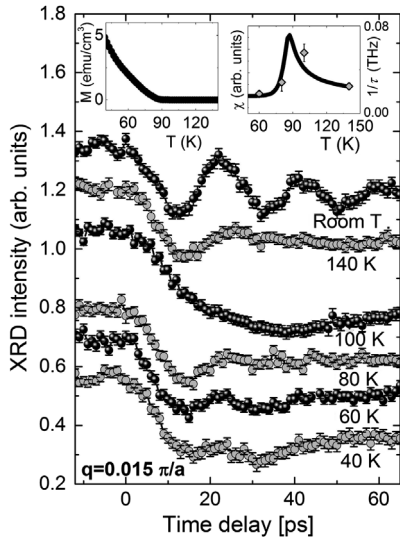
FIG. 2. The temperature dependence of the measured time-dependent diffracted intensities probing the acoustic mode $q = 0.015\ \pi/a$. The data for different temperatures have been shifted along the intensity axis for better visibility. Inset: the measured magnetization curve (left) and, the inverse of the damping time (diamonds, right) and calculated susceptibility (solid line, right) [37].

damping of oscillations (see right inset) is related to the scattering of phonons from spin fluctuations with a cross section scaling as $[T_c/(T - T_c)]^{5/3}$ [41,42].

From Figs. 1(d)–1(f), it is evident that during the first 16 ps following the photoexcitation, the measured data match well with the simulations, indicating that in this time scale, the lattice is still in the state that allows traveling wave normal modes. This observation also implies that the initial excitation of coherent acoustic phonons is provided by the same mechanisms as that at room temperature. The loss of coherence in Figs. 1(e) and 1(f) cannot be explained in terms of phonon-defect and phonon-phonon scatterings, since both processes, having scattering rates that increase with q [43], should affect large q modes instead of small q modes, contrary to our observations.

While at room temperature, the acoustic pulse could be well described in terms of traveling wave normal modes, time-dependent x-ray diffraction measured around and below T_c indicates the transition of the lattice into a disordered state that does not support the propagation of long-wavelength phonon modes. The length-scale dependence of x-ray diffraction waveforms in Figs. 1(d)–1(f) suggests a spatial distortion of the vibrational modes. The reversibility and reproducibility of this effect has been checked by recording each time scan twice and by measuring the same data set at a higher laser fluence. In terms of modeling, the solid cannot be treated as continuum medium. However, a qualitative description that captures the physics observed here can be obtained by considering the equation of motion for acoustic

modes in the presence of a spin-phonon interaction (see Supplemental Material [23], Secs. C and D, which include Refs. [1,35,44–50]),

$$m_j \frac{\partial^2 u}{\partial t^2} = k_\alpha(u_{j+1} - u_j) + k_\beta(u_{j-1} - u_j)$$
$$+ r\Delta k_{\text{mag}}(u_{i+1} - u_j) + r\Delta k_{\text{mag}}(u_{i-1} - u_j). \quad (1)$$

This equation represents a linear chain composed of N masses m_j connected by springs with effective force constants k_α and k_β. Here, m_j stands for the mass of an atom (Ga, As or Mn) in the unit cell (see Supplemental Material [23], Sec. D), u_j denotes the displacement, and k_α and k_β are the effective force constants between the layers $(j, j+1)$ and $(j, j-1)$, respectively. For a host atom $r = 0$, whereas for an impurity atom $r = 1$. The spin-phonon interaction arises due to the modulation of the exchange constant by phonons, and it adds a magnetic contribution $\Delta k_{\text{mag}} \approx -J''(u)\langle \mathbf{S}_0\mathbf{S}_1 \rangle$ to the spring constants of magnetic impurity atoms, with $J''(u)$ being the second derivative of the exchange interaction with the phonon coordinate and $\langle \mathbf{S}_0\mathbf{S}_1 \rangle$ the two-spin correlation function [44]. In (Ga,Mn)As with a nominal Mn doping of 9%, a fraction of Mn is incorporated in interstitial positions [29]. Assuming that interstitial atoms form pairs with substitutional Mn atoms, the partial concentrations of substitutional and interstitial impurities, $x_s \approx 5.5\%$ and $x_i \approx 3.5\%$, respectively (see Supplemental Material [23], Sec. A), yield $x_{s,\text{eff}} = x_s - x_i = 2\%$ uncompensated Mn moments. In contrast to glasses, where a random distribution of spring constants is assumed [14], here we use fixed springs constants that are modified by the spin-phonon interaction only at the Mn atoms. Figure 3 shows the effect of the spin-phonon interaction in the long-wavelength acoustic modes predicted by Eq. (1). In a system that has no ferromagnetic correlations, $\Delta k_{\text{mag}} = 0$, the eigenvectors have a harmonic spatial dependence, thus allowing a single q to be associated with each frequency ω_q, Figs. 3(a) and 3(c). When $\Delta k_{\text{mag}} = -0.018(k_\alpha + k_\beta)/2 \approx -24.7$ meV/Å^2 (i.e., the impurity atoms are ferromagnetically coupled), with $k_\alpha = 25$ N/m and $k_\beta = 19$ N/m obtained by (a) matching the simulated and measured dispersion relations and (b) by setting the zone boundary phonon frequencies $\omega_{LO}(X) - \omega_{LA}(X) = 2\pi(0.4)$ THz (ω_{LO} and ω_{LA} are the longitudinal optical and acoustic phonon frequencies at the X point of the Brillouin zone)[51], low frequency modes are profoundly affected, Figs. 3(b) and 3(d)[52]. The eigenvectors cannot be assigned to a single q but rather should be represented as a superposition of plane waves with different q's, or equivalently, the same frequency is carried by several plane waves with different wave vectors. This happens because the spin-phonon contribution on the spring constants Δk_{mag} alters the inertia of the magnetic impurities. Consequently, the host atoms will adopt a mode
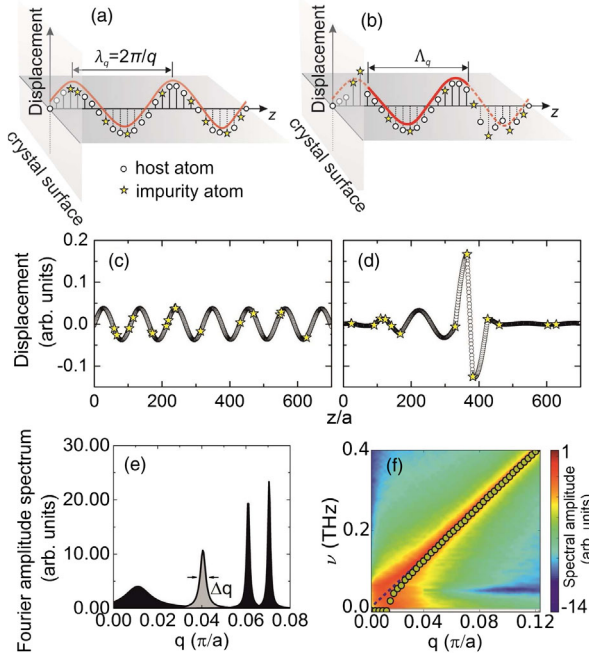
FIG. 3. Eigenvectors of a linear chain of atoms with randomly distributed impurities. Panels (a) and (b) show a schematic drawing of a mode eigenvector without and with magnetic correlation of spins, respectively. In (a), mode eigenvectors can be described by a sinusoidal wave with a well-defined wavelength λ_q. In (b), ferromagnetic coupling of randomly distributed magnetic impurities leads to a destruction of a sinusoidal pattern of a vibrational mode. The average distance between two phase interruptions is represented by the coherence length Λ_q. Panel (c) shows a simulated mode $q = 0.018$ π/a eigenvector without spin-phonon interaction ($\Delta k_{\text{mag}} = 0$), whereas panel (d) displays modification of the mode eigenvector when the magnetic contribution to the spring constants around impurities has been set to $\Delta k_{\text{mag}} = -24.7$ meV/Å^2. Panel (e) shows the Fourier transformation power spectrum of selected acoustic mode eigenvectors, and panel (f) compares the dispersion relation with that of the unperturbed crystal.

pattern that is necessary to balance the forces with neighboring atoms. The Fourier transformation power spectrum of some selected mode eigenvectors averaged over 100 random configurations is shown in Fig. 3(e). As q is decreased, the eigenvectors expand in the reciprocal space, acquire a width Δq, and quasilocalize in the real space. The width of vibrational modes Δq increases monotonically with Δk_{mag} but not with the doping level x (see Supplemental Material [23], Sec. E). A minimum doping level, which considerably affects the periodicity of the vibration modes, is ∼0.5%. Figure 3(f) compares the dispersion relation of a perturbed chain, obtained by mapping the Fourier power spectrum of mode eigenvectors as a function of mode frequency (intensity pot), with the linear relation $\omega_{\text{unpert}}(q) = v_s q$ (blue dashed line). When q-space broadening is neglected, the dispersion curve (filled circles) deviates from the liner relation only for low q modes, whose spatial periodicity is significantly affected.
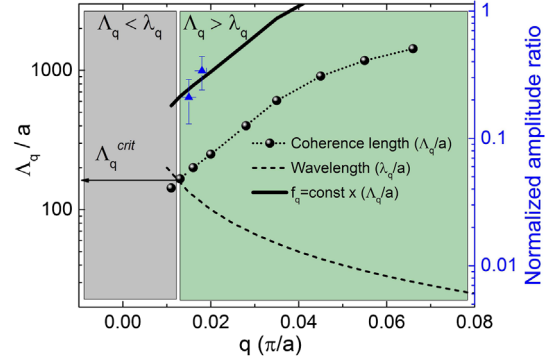

FIG. 4. Simulated coherence length as a function of wave vector q. The critical coherence length Λ_q^{crit} marks the region below which the coherence length of the mode q, Λ_q, is smaller than the wavelength $\lambda_q = 2\pi/q$. In this region phonons cannot sample the periodicity of the lattice and the wave vectors cannot rationalize them anymore. Blue triangles represent the oscillation amplitudes of the x-ray diffraction signal measured at 60 K normalized to those at room temperature. The data corresponding to the acoustic modes 0.018 π/a and 0.015 π/a follow the functional dependence of $\Lambda_q(q)$ multiplied by a constant factor.

Below a cutoff wave vector q_c, the dispersion flattens (the mode frequency becomes imaginary), and the spatial periodicity of the lattice cannot be sampled anymore. In these simulations, we have omitted the reduction of force constants on each side of the interstitials. Different scenarios including various interactions such as force constant reduction and the presence or omission of antisites, are discussed in the Supplemental Material [23], Sec. F, which includes Refs. [1,10,53].

From the widths Δq, we can define the coherence length, $\Lambda_q = 2\pi/\Delta q$, which describes the average distance between two phase interruptions in the mode eigenvector, see Fig. 3(b). A critical coherence length $\Lambda_q^{\text{crit}} \approx 2\pi/q_c$ marks a region below which the coherence length of the mode Λ_q is smaller than the wavelength λ_q, see Fig. 4. When $\Lambda_q < \lambda_q$, phonons see a disordered system and cannot sample the periodicity of the lattice. In this context, the wave vector is not a well-defined quantity anymore. In Fig. 4, we compare the oscillation amplitudes of the x-ray diffraction signal measured at 60 K, normalized to those at room temperature [i.e., $A_q(60 \text{ K})/A_q(300 \text{ K})$]. The data corresponding to the acoustic modes 0.018 π/a and 0.015 π/a follow the functional dependence of $\Lambda_q(q)$. The long wavelength acoustic mode $q = 0.012$ π/a, on the other hand, cannot be assigned to a waveform that would describe coherent oscillation in the x-ray diffraction signal as the wavelength of this mode, $\lambda_q = 2\pi/q = 167a$, is close to the critical coherence length $\Lambda_q^{\text{crit}} \approx 162a$. As a result, this acoustic mode loses its coherence faster than other high-q modes, and in this way, it contributes to a diffusive background rather than to the oscillatory signal, in agreement with our measurements.

In conclusion, our measurements show that in ferromagnetic semiconductors with randomly distributed magnetic impurities, a spin-phonon interaction significantly affects the long wavelength acoustic modes. The length scale dependence of measured x-ray diffraction waveforms cannot be explained by invoking phonon-defect and phonon-phonon scatterings mechanisms that, having rates that increase with decreasing phonon wavelength [43], have less pronounced effects at long wavelength modes. Instead, they can be consistently interpreted in terms of magnetically induced quasilocalization of vibration modes. By altering the inertia of randomly distributed impurity atoms, a spin-phonon interaction destroys the harmonic displacement pattern of long wavelength vibrational modes. This observation will have important implications on many properties of these materials in which the lattice vibrations participate, in particular, in heat transfer, since the quasilocalization of modes contributes to the confinement of thermal energy rather than to its distribution. It will also contribute to the understanding of many physical processes, such as carrier-phonon, impurity-phonon, and phonon-phonon scattering, whose scattering rates are typically estimated by assuming harmonic displacement patterns of normal modes [4,43,54].

---

[*]Corresponding author.
faton.s.krasniqi@web.de

[†]Corresponding author.
yinpeng.zhong@mpsd.mpg.de

[‡]Present address: SwissFEL, Paul Scherrer Institut, 5232 Villigen PSI, Switzerland.

[§]Present address: Institute of Physics, Carl von Ossietzky University Oldenburg, Carl-von-Ossietzky-Strasse 9-11, 26129 Oldenburg, Germany.

[‖]Present address: Physikalisch-Technische Bundesanstalt, Bundesallee 100, 38116 Braunschweig, Germany.

[1] A. S. Barker and A. J. Sievers, Rev. Mod. Phys. **47**, S1 (1975).

[2] A. A. Maradudin, Rep. Prog. Phys. **28**, 331 (1965).

[3] Carrier-phonon and phonon-phonon scattering, which are the most dominant phonon processes that govern the electrical and heat conductivity of semiconductor crystals, are understood and calculated by assuming phonon modes with sinusoidal displacement patterns [4]. A broadening of vibrational modes in the momentum space will affect their transition rate matrices.

[4] B. K. Ridley, *Quantum Processes in Semiconductors* (Oxford University Press, Oxford, 1999), Chap. 3.

[5] T. Dietl and H. Ohno, Rev. Mod. Phys. **86**, 187 (2014).

[6] T. Jungwirth, J. Wunderlich, V. Novák, K. Olejník, B. L. Gallagher, R. P. Campion, K. W. Edmonds, A. W. Rushforth, A. J. Ferguson, and P. Němec, Rev. Mod. Phys. **86**, 855 (2014).

[7] P. B. Allen, J. L. Feldman, J. Fabian, and F. Wooten, Philos. Mag. B **79**, 1715 (1999).

[8] B. B. Laird and H. R. Schober, Phys. Rev. Lett. **66**, 636 (1991).

[9] P. H. Dederichs, C. Lehmann, and A. Scholz, Phys. Rev. Lett. **31**, 1130 (1973).

[10] A. J. Sievers and S. Takeno, Phys. Rev. A **140**, A1030 (1965).

[11] J. M. Larkin and A. J. H. McGaughey, Phys. Rev. B **89**, 144303 (2014).

[12] Y. G. Vainer, A. V. Naumov, M. Bauer, and L. Kador, Phys. Rev. Lett. **97**, 185501 (2006).

[13] W. Schirmacher, G. Diezemann, and C. Ganter, Phys. Rev. Lett. **81**, 136 (1998).

[14] Y. M. Beltukov, V. I. Kozub, and D. A. Parshin, Phys. Rev. B **87**, 134203 (2013).

[15] M. Trigo et al., Nat. Phys. **9**, 790 (2013).

[16] D. Zhu, A. Robert, T. Henighan, H. T. Lemke, M. Chollet, J. M. Glownia, D. A. Reis, and M. Trigo, Phys. Rev. B **92**, 054303 (2015).

[17] M. Chollet et al., J. Synchrotron Radiat. **22**, 503 (2015).

[18] P. Ruello and V. E. Gusev, Ultrasonics **56**, 21 (2015).

[19] A. M. Lindenberg et al., Phys. Rev. Lett. **84**, 111 (2000).

[20] D. A. Reis et al., Phys. Rev. Lett. **86**, 3072 (2001).

[21] F. S. Krasniqi, S. L. Johnson, P. Beaud, M. Kaiser, D. Grolimund, and G. Ingold, Phys. Rev. B **78**, 174302 (2008).

[22] L. Chen, S. Yan, P. F. Xu, J. Lu, W. Z. Wang, J. J. Deng, X. Qian, Y. Ji, and J. H. Zhao, Appl. Phys. Lett. **95**, 182505 (2009).

[23] See Supplemental Material at http://link.aps.org/supplemental/10.1103/PhysRevLett.120.105501 for materials, methods and modeling.

[24] W. E. White, A. Robert, and M. Dunne, J. Synchrotron Radiat. **22**, 472 (2015).

[25] L. Strüder et al., Nucl. Instrum. Methods A **614**, 483 (2010).

[26] K. Y. Wang, M. Sawicki, K. W. Edmonds, R. P. Campion, S. Maat, C. T. Foxon, B. L. Gallagher, and T. Dietl, Phys. Rev. Lett. **95**, 217204 (2005).

[27] P. Němec et al., Nat. Commun. **4**, 1422 (2013).

[28] J. Blinowski and P. Kacman, Phys. Rev. B **67**, 121204 (2003).

[29] T. Jungwirth et al., Phys. Rev. B **72**, 165204 (2005).

[30] M. Sawicki, D. Chiba, A. Korbecka, Y. Nishitani, J. A. Majewski, F. Matsukura, T. Dietl, and H. Ohno, Nat. Phys. **6**, 22 (2010).

[31] M. F. DeCamp, D. A. Reis, D. M. Fritz, P. H. Bucksbaum, E. M. Dufresne, and R. Clarke, J. Synchrotron Radiat. **12**, 177 (2005).

[32] The lattice parameter was estimated by measuring the separation between the (004) Bragg peak of $Ga_{0.91}Mn_{0.09}As$ and that of a thick GaAs crystal with (001) surface orientation, mounted on the same holder and having a well known lattice constant (5.65 Å).

[33] J. Qi, J. A. Yan, H. Park, A. Steigerwald, Y. Xu, S. N. Gilbert, X. Liu, J. K. Furdyna, S. T. Pantelides, and N. Tolk, Phys. Rev. B **81**, 115208 (2010).

[34] C. R. Wie, T. A. Tombrello, and T. Vreeland, J. Appl. Phys. **59**, 3743 (1986).

[35] C. Thomsen, H. T. Grahn, H. J. Maris, and J. Tauc, Phys. Rev. B **34**, 4129 (1986).

[36] A. M. Lindenberg, Ph.D. thesis, University of California (2001).

[37] R. Majlis, *The Quantum Theory of Magnetism* (World Scientific, Singapore, 2000), Chap. 3.

[38] R. Skomski, *Simple Models of Magnetism* (Oxford University Press, Oxford, 2008), Chap. 3.

[39] V. Novák *et al.*, Phys. Rev. Lett. **101**, 077201 (2008).

[40] C. Sliwa and T. Dietl, Phys. Rev. B **83**, 245210 (2011).

[41] H. S. Bennett, J. Phys. (Paris), Colloq. **32**, C1-526 (1971).

[42] As T_c is approached from above, droplets of correlated spins (i.e., islands of ordered spins immersed in a paramagnetic matrix) act as a scattering centers. Below T_c, on the other hand, phonons are scattered from islands of disordered spins immersed in a ferromagnetic matrix.

[43] J. P. Wolfe, *Imaging Phonons* (Cambridge University Press, New York, 1998).

[44] W. Baltensperger and J. Helman, Helv. Phys. Acta **41**, 668 (1968).

[45] K. Wakamura, Solid State Commun. **71**, 1033 (1989).

[46] E. Granado, A. Garcia, J. A. Sanjurjo, C. Rettori, I. Torriani, F. Prado, R. Sanchez, A. Caneiro, and S. B. Oseroff, Phys. Rev. B **60**, 11879 (1999).

[47] C. Wang, G. C. Guo, and L. He, Phys. Rev. B **77**, 134113 (2008).

[48] N. W. Ashcroft and N. D. Mermin, *Solid State Physics* (Harcourt, Orlando, 1976).

[49] M. Herzog, D. Schick, P. Gaal, R. Shayduk, C. Korff Schmising, and M. Bargheer, Appl. Phys. A **106**, 489 (2012).

[50] J. Li, R. Clinite, X. Wang, and J. Cao, Phys. Rev. B **80**, 014304 (2009).

[51] J. S. Blakemore, J. Appl. Phys. **53**, R123 (1982).

[52] Assuming a weak correlation at 60 K, $\langle \mathbf{S}_0 \mathbf{S}_1 \rangle$ between 0.05 and 0.2, $|d^2 J/du^2|$ would lie between 494 meV/Å^2 and 124 meV/Å^2, which is larger than the value predicted for spinel structures, ~ 0.1 meV/Å^2 [55], but of the same order of magnitude as that deduced for the antiferromagnetic compound LaMnO$_{3+\delta}$, ~ 217 meV/Å^2 [46].

[53] J. Mašek, J. Kudrnovsky, and F. Maca, Phys. Rev. B **67**, 153203 (2003).

[54] P. L. Taylor and O. Heinonen, *A Quantum Approach to Condensed Matter Physics* (Cambridge University Press, Cambridge, 2002).

[55] C. J. Fennie and K. M. Rabe, Phys. Rev. Lett. **96**, 205505 (2006).